American Industrial Hygiene Association Journal

ISSN: 0002-8894 (Print) (Online) Journal homepage: https://www.tandfonline.com/loi/aiha20

Evaluation of Algorithms for Tomographic Reconstruction of Chemical Concentrations in Indoor Air

L. Todd & G. Ramachandran

To cite this article: L. Todd & G. Ramachandran (1994) Evaluation of Algorithms for Tomographic Reconstruction of Chemical Concentrations in Indoor Air, American Industrial Hygiene Association Journal, 55:5, 403-417, DOI: 10.1080/15428119491018844

To link to this article: https://doi.org/10.1080/15428119491018844

Published online: 04 Jun 2010.

Evaluation of Algorithms for Tomographic Reconstruction of Chemical Concentrations in Indoor Air

L. Todd
G. Ramachandran

University of North Carolina, Department of Environmental Sciences and Engineering, C.B. 7400, Chapel Hill, NC 27599

Numerical studies were performed to evaluate and compare four different algorithms for tomographically reconstructing pollutant concentrations in indoor air measured with an optical remote sensing system. With a remote sensing/computed tomography system, two-dimensional maps of air concentrations can be created for an entire room with good spatial and temporal resolution. The success of such a system for characterizing the flow of contaminants in air, exposure assessment, and leak detection depends on the choice of tomographic reconstruction algorithm. A systematic method was developed to evaluate the performance of four algorithms: ART, ART3, SIRT, and SART. One hundred and twenty test maps were reconstructed by each algorithm under ideal and nonideal sampling conditions, and image quality was evaluated using four criteria. The nonideal sampling conditions included simulation of measurement noise and reduction in the number density of rays. Performance of the algorithms was found to be intimately related to the number of peaks in the test maps. The importance of using multiple measures of image quality was underscored by the fact that for some sampling conditions simulated, performance of the algorithms was judged differently depending on the evaluation criteria. Results indicated that using numerical studies is successful for evaluating such algorithms.

Currently, indoor air is sampled for chemical contaminants by point samplers that average concentrations over time. The samplers are placed on a few individuals for exposure assessment or in specific locations for area concentration profiles, and the results are assumed to be representative of the larger work force or entire room. This assumption may not be valid; in practice, it is difficult to select a representative subset of individuals or locations to sample because the concentration distributions are unknown.

One strategy for selecting the subset of individuals involves an observational approach that incorporates both task similarities and similarities of the local environments where the individuals spend their time; they are both strong determinants of exposure.[1] Task similarity may be predicted from interviews and direct observation of individuals; however, environmental similarity is much more difficult to predict. Supporting data on ventilation systems and air flow patterns for an entire room are usually lacking. Therefore, the individuals selected for sampling may not truly be representative.

Alternative sampling strategies involve statistical sampling that uses the results from measurements from a large data set to classify workers. The effort expended in observational detail is minimized in lieu of maximizing data collection.

Strategies for selecting locations for area sampling assume that those with the highest or most relevant concentrations are represented and that the areas between the samplers are of less importance. In practice, this assumption is difficult to support. An accurate and representative profile of air contaminant concentrations cannot usually be constructed; the industrial hygienist is left with isolated numbers that provide poor spatial resolution of chemical concentrations for a room. Whether used for personal or area sampling, point samplers such as passive dosimeters and solid adsorbents average concentrations over time, effectively smoothing out fluctuations, which results in poor temporal resolution of chemical concentrations.

A method has been proposed that can create two-dimensional maps of chemical concentrations in air for an entire room and provide accurate spatial and temporal information about the concentration and flow of air contaminants.[2] This method combines the real-time chemical detection methods of optical remote sensing with the mapping capabilities of computed tomography. The optical remote sensing system

This project was supported by grant 1 K01 OH00103-01 from the National Institute for Occupational Safety and Health of the Centers for Disease Control, by the Kenan Foundation Fellowship at the University of North Carolina, and by the U.S. Environmental Protection Agency cooperative agreement CR815152 with the University of North Carolina.

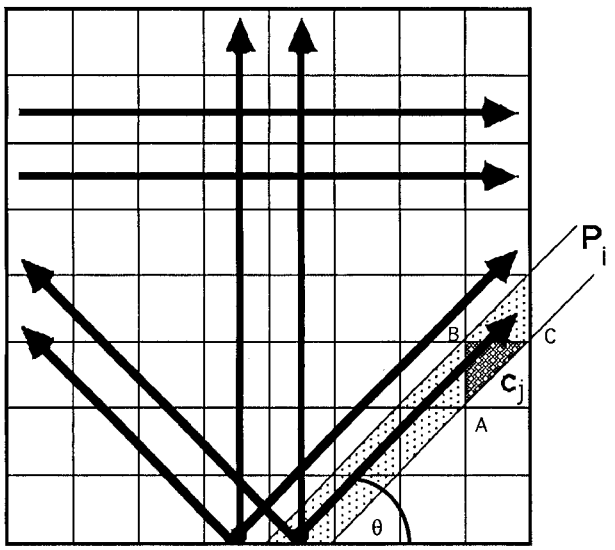

FIGURE 1. Geometry of an equal-angle, parallel-projection configuration. Representation of an 8 × 8 room with four projection angles, 0°, 90°, and ± 45°. θ is the projection angle; c_j is the concentration within the jth cell; p_i is the ith ray sum; ABC is the area of the jth cell intercepted by the ith ray.

scans the room and each real-time measurement provides a path-integrated concentration, not a point sample. Using a tomographic reconstruction algorithm, a computer uses these measurements to reconstruct a two-dimensional chemical concentration map of the entire room in a few minutes. Such concentration maps can be used to track the flow patterns of air contaminants in an entire room and provide detailed information about the spatial domain of the worker. This local environment of the worker defines a region of importance for exposure assessment.

The maps can be used to help choose a truly representative subset of workers to use with point-sampling methods. If the maps are coupled with worker location information, they can be used directly to evaluate exposure for a much larger number of workers than currently possible using point-sampling methods. The ability to obtain measurements for days, weeks, or months would facilitate the determination of exposure variability.

The use of a single optical remote sensing beam for detecting gases and vapors has been primarily examined for the outdoors.[3,4] However, the indoor application is gaining attention.[5] The use of computed tomography and multiple optical remote sensing beams in the workplace was introduced and described in a previous paper.[2] The appropriate choice of a tomographic reconstruction algorithm and a configuration for the placement of the optical remote sensing equipment is essential to the successful implementation of this method.

This article reports on numerical studies to evaluate and compare four different algorithms for tomographically reconstructing pollutant concentrations in indoor air. The evaluation of optical remote sensing configurations will be presented in a subsequent paper.

THEORY AND METHODOLOGY

Evaluation of Reconstruction Algorithms

Over the past 25 years, many tomographic reconstruction algorithms have emerged to solve the problem of reconstructing objects from their projections. These algorithms have been applied in a variety of disciplines including medicine,[6] radio astronomy,[7] electron microscopy[8] and air pollution.[9] The performance of an algorithm has been found to depend on the application, including the types and complexity of the images to be reconstructed, the method of data collection, the number of data samples, and the accuracy of the collected data.[10,11] Therefore, prior to using an algorithm, it should be evaluated through exhaustive numerical studies specific to the application. A thorough evaluation of reconstruction algorithms should incorporate a diversity of appropriate test data, a variation in the number of optical rays to study the effects of under-sampling, and various levels of measurement noise.[10,11]

For this study, computer programs were developed to evaluate different algorithms for reconstructing chemical concentrations indoors. For each algorithm, 120 test concentration maps were reconstructed under ideal and nonideal sampling conditions; the nonideal conditions included a reduced number density of sampling rays, and three levels of measurement noise.

Reconstruction Algorithms

Many types of tomographic algorithms have been developed. The three that have been explored in the greatest depth include analytic,[12,13] back-projection,[14,15] and iterative methods.[6,7,16] When evaluated for other applications, the methods have been found to differ in computational speed, allowable configurations, and performance with measurement noise and limited data. Iterative methods were chosen for analysis in this study because they allow flexibility in the placement of the remote sensing equipment in a room, perform well with limited data, and allow constraints to be imposed on the reconstructed measurements.[17,18] These attributes are important for reconstructing chemical concentrations indoors where there will, undoubtedly, be limitations on the quality and quantity of usable data.

The four iterative algorithms selected were ART (Algebraic Reconstruction Technique),[10,16] ART3,[19,20] SIRT (Simultaneous Iterative Reconstruction technique),[15,21] and SART (Simultaneous Algebraic Reconstruction Technique).[22–24] ART has been used in previous research on reconstructing chemical concentrations in air.[2] ART3, SIRT, and SART were chosen because they all have been reported to perform better than ART in the presence of noise.[20,23]

To evaluate these algorithms, an idealized room is broken into an N × N grid of cells. Figure 1 shows a room as an 8 × 8 grid. Within each cell the concentration c_j is assumed to be uniform and non-negative. The acute angle that a light

ray makes with the room width is called the projection angle, and all rays at the same angle constitute a projection. Ray sums are line integrals of c along various paths through the room. The i^{th} ray sum is denoted by p_i. The relationship between the c_j's and the p_i's is approximated as a strip sum, see Equation 1.

$$p_i = \sum_{j=1}^{N^2} a_{ij}\, c_j,\ i = 1,\ 2,\ \ldots\ M, \qquad (1)$$

where M is the total number of rays and a is the weighting factor that represents the contribution of the j^{th} cell to the i^{th} ray sum. This contribution is equal to the fractional area of the j^{th} cell intercepted by the i^{th} ray, i.e., the area of the triangle ABC, in Figure 1.

ART Algorithm

For ART, an initial guess is made at the values of all the cells in the grid; based on this guess, the first ray sum is calculated. The values of all the cells are then corrected so that the calculated ray sum equals the measured ray sum. The correction procedure is shown in Equation 2, and is repeated sequentially for each ray. One iteration is completed when all the ray sums have been corrected.

$$c_j(q+1) = c_j^{(q)} + \frac{\left(p_i - \sum_{j=1}^{N^2} a_{ij}\, c_j\right) a_{ij}}{\sum_{j=1}^{N^2} a_{ij}^2},\ i = 1,\ 2,\ 3,\ \ldots\ M \qquad (2)$$

where q is the iteration number.

ART3 Algorithm

A precise solution to Equation 1 is generally impossible because the p_i's are physical measurements and are usually noisy; ART3 takes this into consideration by finding a solution to the inequalities shown in Equation 3 using the same correction scheme as in Equation 2. The equations have to be satisfied only within a tolerance, which should be estimated from a knowledge of the experimental conditions and the expected error.

$$p_i - \varepsilon_i \le \sum_{j=1}^{N^2} a_{ij}\, c_j \le p_i + \varepsilon_i,\ i = 1,\ 2,\ 3,\ \ldots\ M, \qquad (3)$$

where ε_i is an allowed tolerance.

SIRT Algorithm

This algorithm also uses Equation 2 to determine the change in the jth cell; however, the value is not changed immediately. At the end of each iteration, the cell values are changed after calculating changes for all the ray sums. The change for each cell is equal to the average value of all the corrections made to that cell.

SART Algorithm

In SART,[22–24] the corrections are made as in SIRT, except that instead of waiting to go through all the ray sums, average corrections are applied to each cell after calculations are made for all ray sums in one projection. Therefore, when four projection angles are used, four averages are applied to each cell in an iteration. In this algorithm ray integrals are calculated instead of strip integrals. Each ray integral is approximated as a finite sum involving M_i equidistant points along the ray, see Equation 4.

$$p_i = \sum_{m=1}^{M_i} \underline{c}(s_{im})\Delta s, \qquad (4)$$

where Δs is the stepsize that was chosen to be half the grid cell width, and $\underline{c}\,(s_{im})$ is determined from the values of c_j of the neighboring cells by bilinear interpolation,[22] see Equation 5.

$$\underline{c}(s_{im}) = \sum_{j=1}^{N^2} d_{ijm}\, c_j,\ \text{for } m = 1,\ 2,\ \ldots\ M_i, \qquad (5)$$

where the coefficient d_{ijm} is the contribution made by the j^{th} cell to the m^{th} point in the i^{th} ray.

Stopping Criteria for Iterative Process

The stopping criteria for all four algorithms were based on the fractional change in the variance of the reconstructed concentration map, from one iteration to the next, see Equation 6.[19,25] The iterations were stopped when this fractional change was smaller than 0.001 for both ideal sampling conditions and nonideal sampling conditions that used a reduced number of rays. When simulated measurement noise was added, the stopping criteria was relaxed to 0.01. Noise causes inconsistencies in the projection data that may make it impossible to converge and satisfy a small variance difference.

$$\left|\frac{\text{Variance}(q+1) - \text{Variance}(q)}{\text{Variance}(q)}\right| < \text{Stopping Value}$$

$$\text{Variance}(q) = \frac{\sum_{j=1}^{N^2} \left(c_j - c_{avg}\right)^2}{N^2}, \qquad (6)$$

where q is the qth iteration number, c_j is the estimated value of the jth element in the map of N^2 cells, and c_{avg} is the mean concentration of the true values in the concentration map.

The number of iterations required to reach the stopping criteria was used as a measure of convergence rate.

Test Remote Sensing Configurations

An equal angle parallel projection configuration, Figure 1, was used in evaluating the performance of the algorithms.[2] The hypothetical cross section of a room was broken into a 40 × 40 grid of cells. Four projections were used for the reconstructions: 0, 90, and ± 45 degrees. Using only

four projections, with a total of 240 rays, to reconstruct 1600 grid cells results in a system of equations that is highly underdetermined. However, numerical simulations using this configuration for reconstructing chemical concentrations found four projections to be sufficient to achieve good reconstructions assuming Gaussian profiles.[2] This configuration was selected for evaluating reconstruction algorithms because every grid cell has the same number and orientation of rays going through it; the location of the peaks in the test concentration maps has no affect on the quality of the reconstructions. Therefore, differences in the reconstructions should be directly related to the algorithm.

Test Concentration Maps

Test concentration maps used to evaluate the algorithms should be representative of the wide variety of concentration profiles in the workplace. The number of test maps must be large enough to obtain a statistically meaningful sample.[11] To ensure diversity and eliminate human bias, a computer was used to randomly generate 120 different maps. The test maps assumed a 40 × 40 room with grid cell locations described by a Cartesian coordinate system. Normal bivariate distributions were used to model concentrations. The maps had from 1 to 6 randomly located concentration peaks; peak heights varied randomly from 50 to 500 ppm, and peak standard deviations varied randomly from 1 to 6. The number of peaks in a map was taken as a measure of the complexity of the map. The set of 120 test maps included 20 maps for each of the 6 levels of complexity. Simulated ray measurements were made from the test concentration maps and the algorithms were then used to reconstruct the maps from these simulated measurements.

Test Sampling Conditions

Ideal sampling conditions were used to establish a baseline for comparing the algorithms. Ideal sampling assumes that a full complement of contiguous rays is used for each of the four projections in the equal angle parallel projection configuration and that the data is free of measurement noise. The 120 maps that were reconstructed by each algorithm represented the "best possible" reconstructions using this configuration with four projections. For the ideal case, the ART3 algorithm is mathematically equivalent to ART; the baseline values for ART are the baseline values for ART3.

The concentration maps were then reconstructed under nonideal sampling conditions that included a reduction in the number density of rays and the addition of simulated measurement error. To investigate the effect of reduced number density of rays (under-sampling) on reconstruction accuracy, all 120 test maps were reconstructed using 50% and 25% of the full complement of rays. The number density of rays was reduced systematically; for the 50% case, every other ray was deleted, while for the 25% case, three out of every four rays in a projection were deleted. At the start of the reconstruction, the missing rays were assigned values based on a cubic spline interpolation of the adjacent ray sums.

Noise was simulated by adding normally distributed random errors with a mean of zero and standard deviations of 5%, 10%, and 20% to the ray sums before reconstruction. Sixty concentration maps were used to evaluate the effect of measurement noise. For each test map, 10 simulations were performed at each of the three noise levels, resulting in a total of 1800 reconstructions in the presence of noise.

Evaluating Quality of Reconstruction

For industrial hygiene, the quality of the reconstructed test concentration map determines the ability to use the map for exposure assessment, leak detection, and evaluating air flow of contaminants. No single statistical measurement can be used exclusively to compare mathematical algorithms. For this research, both quantitative and qualitative measures were used to evaluate image quality. Two of the quantitative measures, nearness and projection data distance, have been used in other applications.[19,25,26] The third quantitative measure, exposure location analysis, was developed for the industrial hygiene application[2,27] and is similar to the idea of resolution described by Frieder and Herman.[28] The qualitative measure, visual assessment of the two-dimensional reconstruction maps, is important for all applications of tomography.

Nearness, Equation 7, describes the discrepancy between the original concentration map and the reconstructed concentration map.[19,25] Nearness evaluates errors over all the grid cells in a map; a nearness of zero implies a perfect match. Nearness is a dimensionless number.

$$\text{Nearness} = \frac{\sqrt{\sum_{j=1}^{N^2}\left(c_j^* - c_j\right)^2}}{\sqrt{\sum_{j=1}^{N^2}\left(c_j^* - c_{avg}^*\right)^2}}, \qquad (7)$$

where c_j^* is the true value for the jth cell in the map, c_j is the estimated value for the jth cell in the map, and c_{avg}^* is the mean true concentration in the map.

Projection data distance, Equation 8, is a measure of how closely the reconstructed ray sums match the original ray sums.[19,26] A data distance value of zero implies a perfect match. Data distance has units of concentration times pathlength, e.g., ppm-m.

$$\text{Projection Data Distance} = \frac{\sqrt{\sum_{i=1}^{M}\left(p_i - \sum_{j=1}^{N^2} a_{ij}\, c_j\right)^2}}{M}, \qquad (8)$$

where p_i is the true i^{th} ray sum, $\sum_{j=1}^{N^2} a_{ij}c_j$ is the calculated i^{th} ray sum, a_{ij} is the contribution of the j^{th} cell to the i^{th} ray, and M is the total number of rays.

Exposure location error analysis gauges how accurately a reconstructed concentration map measures exposure. Assuming that a worker is usually mobile throughout a workday, the cumulative dose of an air toxic that a worker

receives is related to the average exposure over all the locations in the room through which the worker travels. If the room is broken up into a grid of cells as in Figure 1, the accuracy of one specific grid cell in the reconstructed concentration map may not be as important as the average accuracy over all the grid cells visited by a worker. This measure of reconstruction quality is calculated by obtaining the average concentrations for several locations in the original test map and comparing them with the average concentrations for the same locations in the reconstructed map.

For the exposure location error analysis two measurements were computed: the first used peak-centered and the second used randomly selected locations. The peak-centered measurement is a worst case analysis; it averages concentrations at the peak heights, and assumes that an individual spends his or her time at these places of highest concentration in the room. The randomly selected location measurement assumes the individual could work anywhere in the room. For this measurement the computer randomly selected 3, 5, and 10 different locations from the 1600 grid cells. This was repeated 10 times for each location set. Because an individual will usually occupy several grid cells when working at any single location, each location was given two "footprint" sizes, 3 × 3 and 5 × 5. Separate calculations of exposure location error were made for the two footprint sizes, see Equation 9.

$$\text{Exposure Location Error} = \left| \frac{\sum c_n^* - \sum c_n}{\sum c_n^*} \right| \times 100 \quad (9)$$

where c_n^* is the true value for the n^{th} cell of a footprint, c_n is the estimated value for the n^{th} cell of a footprint, and the summations are over all the cells in a footprint.

Visual Assessment

The reconstructed maps were compared visually to the original concentration maps and to each other. The factors that were considered included preservation of peak heights and shapes, location of peaks, smoothness of peaks, and introduction of artifacts.

RESULTS AND DISCUSSION

Ideal Sampling Conditions

Nearness and Data Distance

For all four algorithms the nearness values increased (deteriorated) as the number of peaks in the test maps increased. Figure 2 is a plot of nearness versus number of peaks for the algorithms; the nearness values for the algorithms were statistically different from one another ($p < 0.0001$). For any specific number of peaks in the test maps, ART (and ART3) had the smallest (best) nearness values, SART had slightly higher nearness values, and SIRT had the highest (worst) nearness values. The results for the data distance measurement were similar to the nearness results.

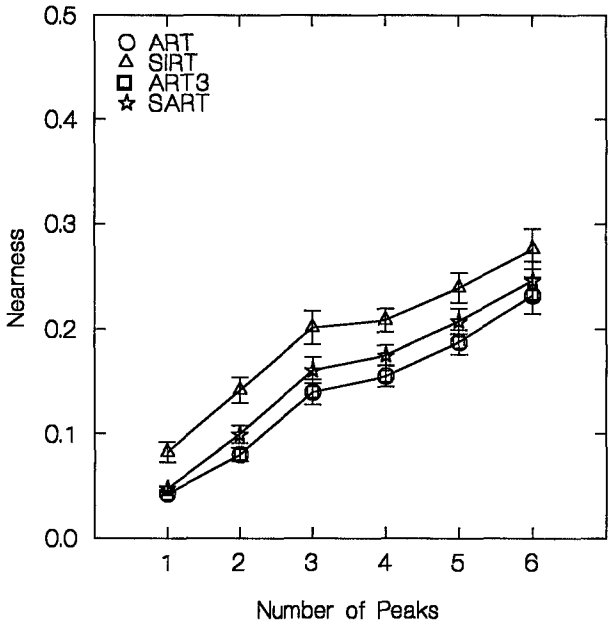

FIGURE 2. Variation of final nearness values with complexity of picture (number of peaks) for the four algorithms in the ideal case; error bars denote one standard error

Number of Iterations

The number of iterations necessary to reach convergence for ART (and ART3) and SART was not dependent on the number of peaks in the test maps, i.e. the complexity of the maps. For SIRT, however, the number of iterations required for convergence decreased with an increase in the number of peaks. The mean number iterations required for convergence was 15 for ART (and ART3), 40 for SART, and 90 for SIRT. ART had the most rapid convergence rate based on number of iterations. Although SIRT took the most iterations, SART is computationally the most expensive algorithm, and the time for convergence of SIRT and SART was similar.

Exposure Location Analysis

Figure 3 is a plot of the mean percent errors for the peak-centered exposure location measure versus the number of peaks in the test maps. As the number of peaks in the test maps increased, the mean percent peak errors increased for all algorithms. As with the other quantitative measures, the ART (and ART3) algorithms produced the smallest errors, the SART algorithm errors were slightly higher, and the SIRT algorithm had the highest errors. The mean percent errors across the algorithms were significantly different from one another ($p < 0.05$).

For all four algorithms the peak-centered exposure values in the original maps correlated well with the peak-centered exposure values in the reconstructed maps. This implies that all the algorithms reconstructed the test maps with good resolution. For all algorithms the correlation was

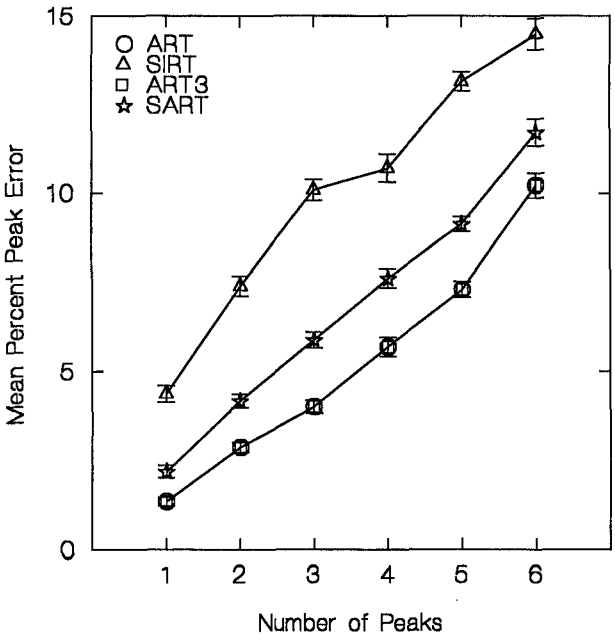

FIGURE 3. Variation of mean percent error in peak value with complexity of picture (number of peaks) for the four algorithms in the ideal case; error bars denote one standard error

similar for test maps with 1 to 5 peaks; at 6 peaks, the increased complexity of the maps translated into decreased correlation. The regression lines produced for all the algorithms were similar to one another. The agreement was good, with the R^2 values above 0.990 for test maps with fewer than six peaks; the correlation dropped at the six-peak level for all algorithms to a low of 0.96 (see Table I). The slopes of all of the regression lines were significantly smaller than 1 ($p < 0.05$), implying an underestimation of exposures.

For the analysis using the randomly selected locations, similar results were obtained with all four algorithms. The correlation between the exposure values calculated in the original maps and the reconstructed maps with the randomly selected locations was better than the correlation obtained with the peak-centered locations for the test maps with six peaks (see Table I). For the ART (and ART3) algorithm, the slopes of all the regression lines were not significantly different from one. For the SIRT algorithm the slopes of the regression lines were not significantly different from one for the maps with less than 6 peaks; for maps with 6 peaks the slope of the regression line was significantly smaller than 1. For the SART algorithm, the slopes of all the regression lines were significantly smaller than 1; the exposures were underestimated. Based on this measure, SART appears to smooth out the images and thus decrease peak values more than the other algorithms.

Visual Image Quality

For all four algorithms the final maps were close in appearance to the original maps and to one another. Using one of the three-peak maps as an example, Figure 4a shows the original map, and 4b, 4c and 4d the reconstructed test maps for ART (and ART3), SIRT, and SART. These represent the "best possible" reconstructions for these algorithms using the equal angle configuration with four projection angles. For all the algorithms, the reconstructed peaks were in their correct locations. All the algorithms tended to smooth out the image; this resulted in shortened peak heights for the tallest peak at location (11, 10), and the sharpest peak at location (7, 32). This is because of the correction schemes used by all the algorithms, which tend to smooth out images and flatten the peaks. The reconstruction using SIRT shortened the peaks more than the other algorithms. All the reconstructions introduced some artifacts at the bases of the peaks, the points of lowest concentration in the map. The extent of shortening of peaks and presence of artifacts would be decreased if more projection angles were used.[2] Based on visual assessment, ART (and ART3) had slightly better reconstructions than the other algorithms, followed by SART and SIRT.

Nonideal Sampling Conditions: Reduced Number Density of Rays

Nearness

For all four algorithms, when only 50% of the rays were used, the nearness values increased in most cases as the number of peaks in the test maps increased (see Figure 5). The nearness values for ART were smaller (better) than for the other algorithms, ART3 had the next smallest nearness values, followed by SIRT and SART. There was no significant difference between the nearness values for the ideal case and when only 50% of the rays were used for ART and SIRT; however, there was a significant difference for ART3 and SART.

TABLE I. R^2 Values for Exposure Values for the Original and Reconstructed Maps for the Four Algorithms for Different Number Density of Rays

		Ideal		*50% rays used*		*25% rays used*	
Algorithm	*# Peaks*	*Peak*	*Random*	*Peak*	*Random*	*Peak*	*Random*
ART	1—5	0.99	0.99	0.99	0.99	0.97	0.99
	6	0.96	0.97	0.96	0.97	0.94	0.95
ART3	1—5	0.99	0.99	0.99	0.99	0.98	0.99
	6	0.96	0.97	0.96	0.97	0.94	0.95
SIRT	1—5	0.99	0.99	0.99	0.99	0.97	0.98
	6	0.96	0.97	0.95	0.97	0.97	0.95
SART	1—5	0.99	0.99	0.97	0.99	0.97	0.99
	6	0.96	0.98	0.96	0.97	0.89	0.96

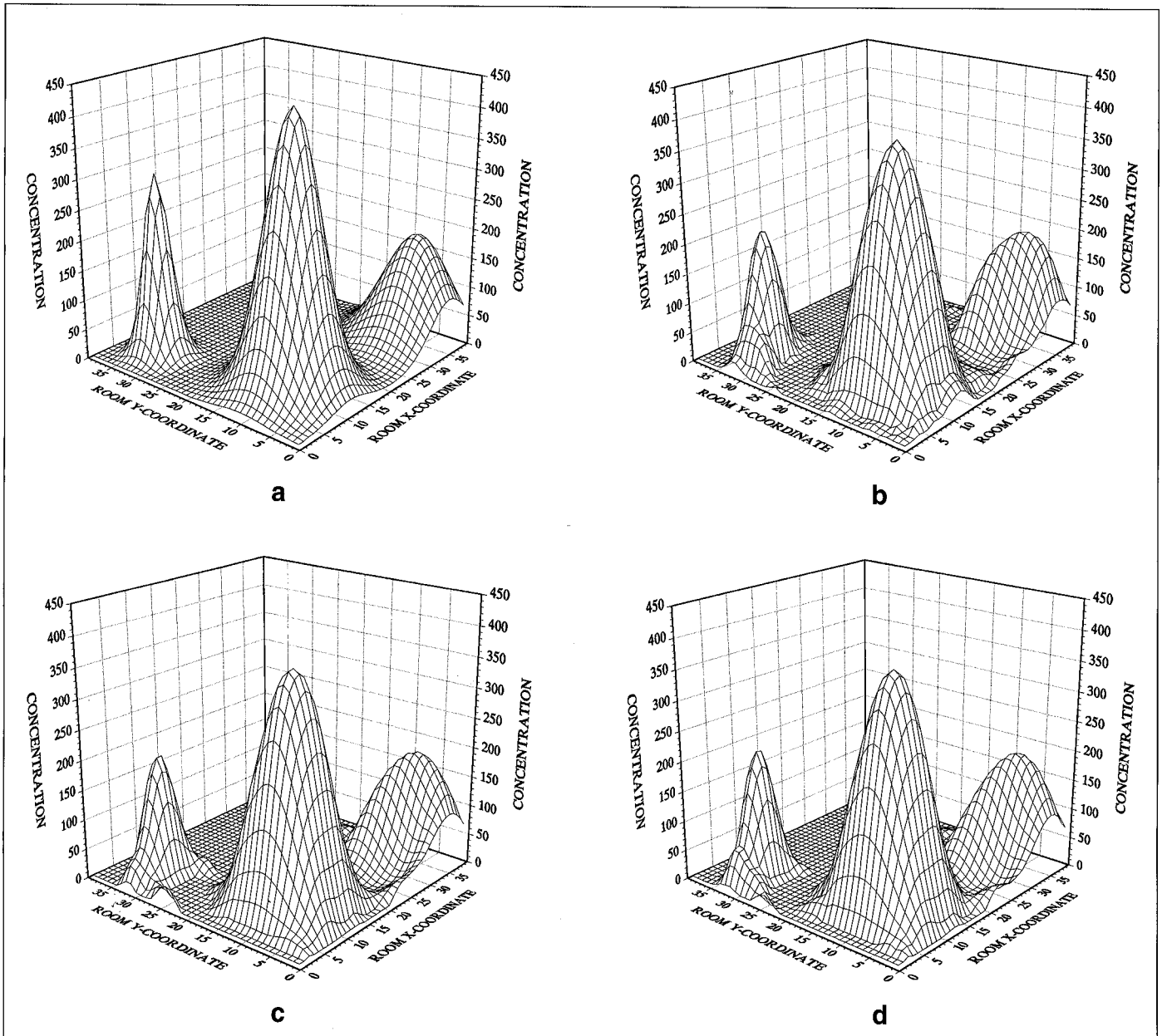

FIGURE 4. (a) Original test map; reconstruction in the ideal case using (b) ART and ART3; (c) SIRT; and (d) SART.

When 25% of the rays were used, the nearness values for all the algorithms were significantly higher than the nearness values when 50% of the rays were used. The nearness values for the four algorithms were not significantly different from each other and were all equal to ~0.3, regardless of the number of peaks in the test maps.

As the number of peaks in the test maps increases above three, the nearness values are not changed as much as those maps with fewer peaks. This is because the concentration patterns tend to be more homogeneous with increasing number of peaks, and as a result, errors in interpolation between rays decrease.

Data Distance

Figure 6 is a plot of data distance versus the number of peaks in the test maps when 50% of the rays were used. As with the ideal case, the data distance values increased with an increase in the number of peaks in the test maps. When 50% of the rays were used, the ART algorithm had the smallest data distance values. There was no significant difference in these values when compared with the ideal. ART3 and SIRT had data distance values significantly higher than ART though not significantly different from one another. The data distance values for SIRT were not significantly different from the ideal case. The data distance values for SART were significantly higher than the ideal case, and the values for the other algorithms ($p < 0.0001$).

When 25% of the rays were used, all of the data distance values for the four algorithms were significantly higher than when 50% of the rays were used ($p < 0.0001$). The order of algorithms from smallest (best) to largest (worst) data distance values rearranged to SIRT, ART, SART, and ART3.

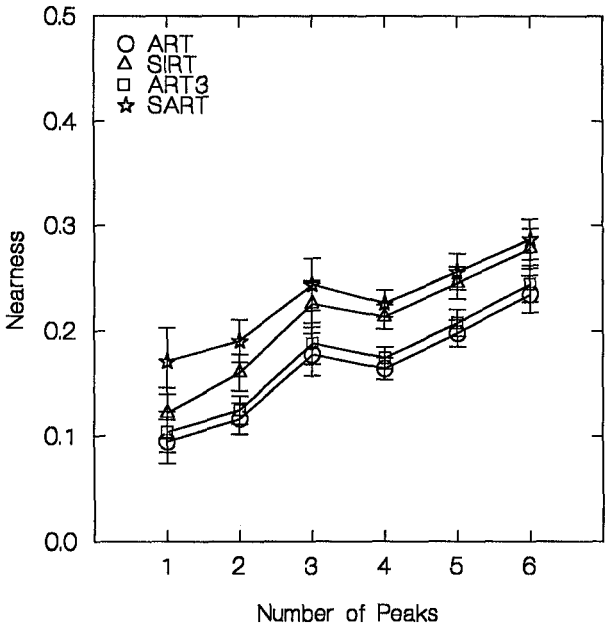

FIGURE 5. Variation of final nearness value with complexity of picture (number of peaks) for the four algorithms when 50% of the rays are used; error bars denote one standard error

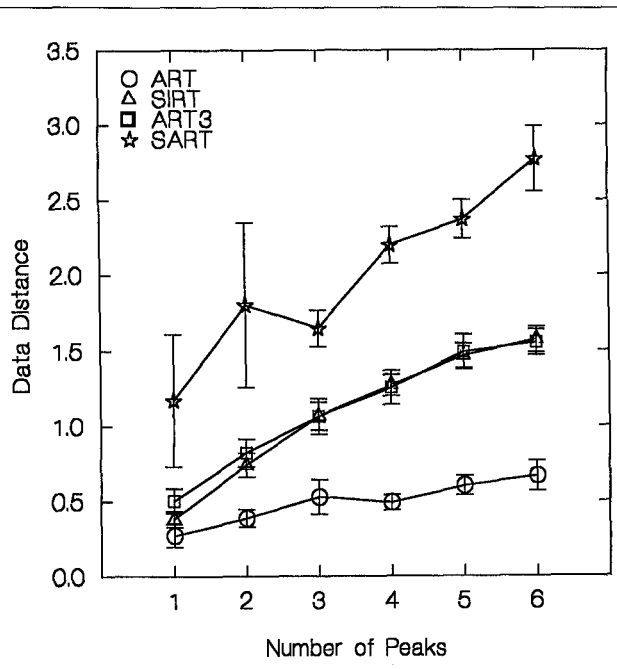

FIGURE 6. Variation of final value of data distance with complexity of picture (number of peaks) for the four algorithms when 50% of the rays are used; error bars denote one standard error

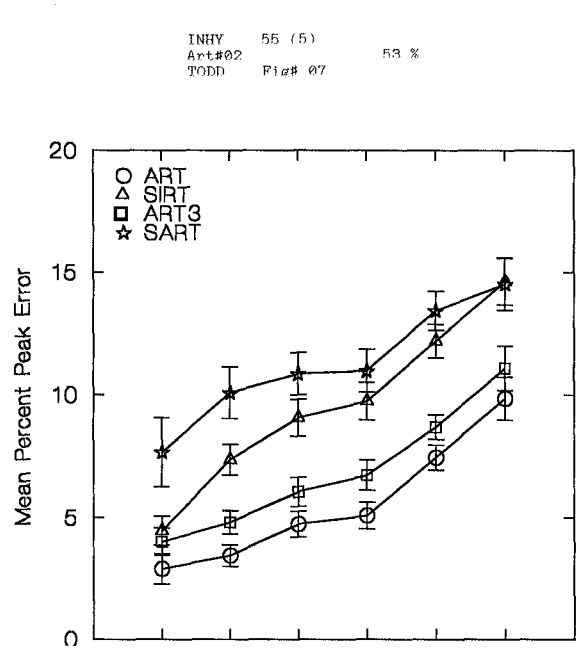

FIGURE 7. Variation of mean percent error in peak value with complexity of picture (number of peaks) for the four algorithms when 50% of the rays are used; error bars denote one standard error

It is not surprising that ART3 had the largest data distance values. This algorithm only requires that the ray sums be matched within a tolerance, unlike the other algorithms, which require exact matching.

Number of Iterations

Except for SART there were minimal changes in the number of iterations required for convergence when fewer rays were used. When 50% of the rays were used, the number of iterations required for convergence decreased for all the algorithms to ~10 for ART, ART3, and SART, and to ~80 for SIRT, regardless of number of peaks in the test maps. When 25% of the rays were used, the number of iterations required for convergence increased to ~20 for ART, ART3, and SART, and to ~90 for SIRT.

Exposure Location Analysis

Figure 7 is a plot of mean percent peak errors for the peak-centered exposure location measure versus the number of peaks, for all four algorithms when 50% of the rays were used. As the number of peaks in the maps increased, the mean percent peak errors increased. When 50% of the rays were used, these errors increase significantly compared to the ideal case only for the SART algorithm ($p < 0.0001$). There was no significant difference between SIRT and SART or between ART and ART3. ART and ART3 gave the best results.

When 25% of the rays were used, the mean percent errors increased significantly for all four algorithms ($p < 0.0001$) compared to when 50% of the rays were used. At this level there was no significant difference between the

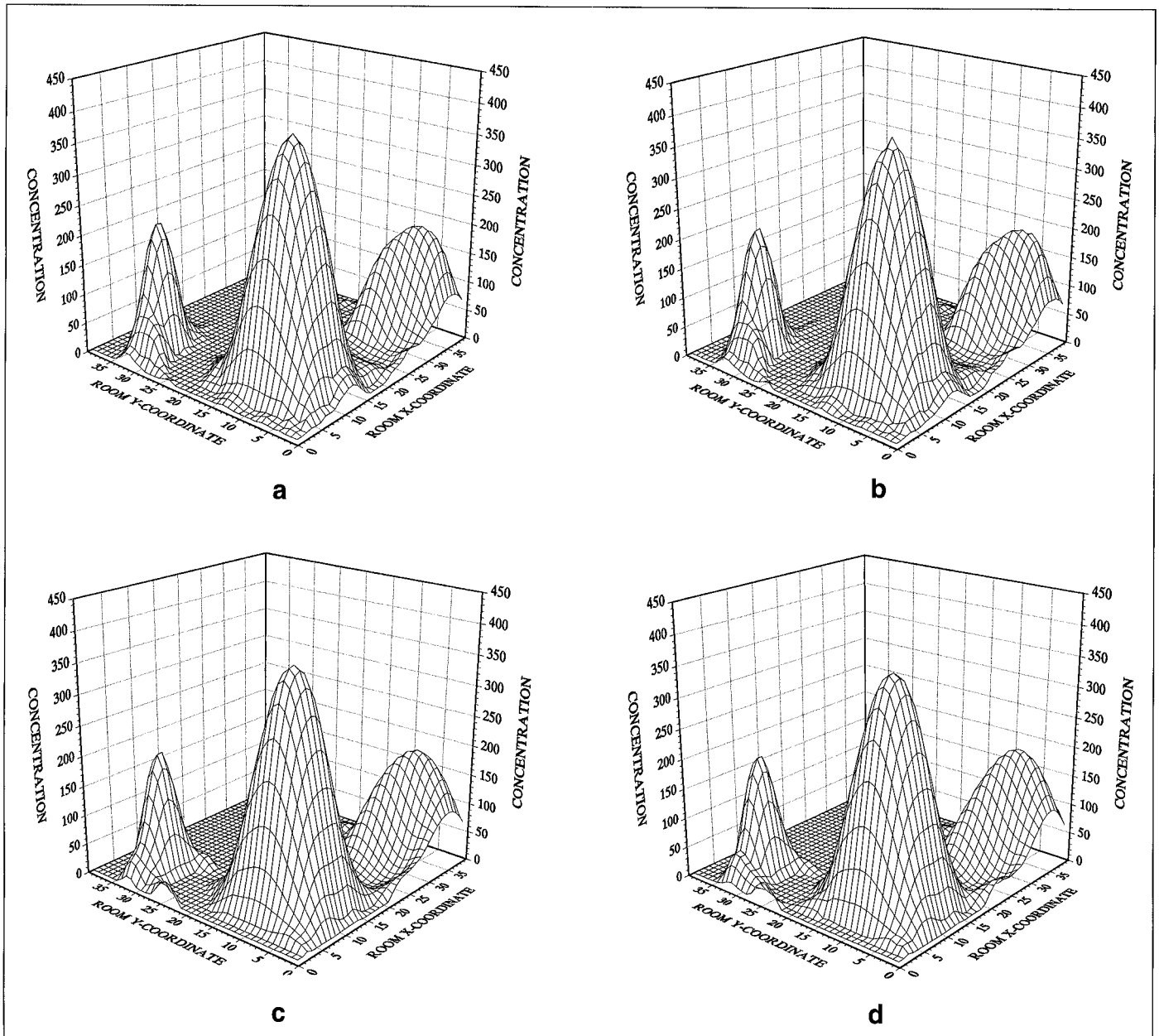

FIGURE 8. Reconstruction when 50% of the rays are used with (a) ART; (b) ART3; (c) SIRT; and (d) SART.

algorithms; the mean percent errors were all about 16% regardless of the number of peaks in the test maps.

Table I shows the R^2 values for the exposure values for the peak-centered and randomly selected locations. For all four algorithms, the peak-centered exposure values for the original maps correlated well with the peak-centered exposure values for the reconstructed maps when 50% of the rays were used. The R^2 values were not significantly different than the R^2 values for the ideal case, implying no loss in resolution.

When 25% of the rays were used, the R^2 values dropped. The R^2 values for ART, ART3, and SIRT were similar to one another; the correlation was the poorest for SART. As with the ideal case, the slopes of the regression lines for the peak-centered errors for all the algorithms when 25% or 50% of the rays were used were all significantly less than 1 ($p < 0.05$).

The correlation between the exposure values in the original and the reconstructed maps was slightly better for the randomly selected locations than for the peak-centered locations when 50% or 25% of the rays were used. For ART, ART3, and SIRT, the slopes of all the regression lines were significantly larger than 1 ($p < 0.05$); the exposures were overestimated. As with the ideal case, the slopes of the regression lines for the SART algorithm were significantly smaller than 1 ($p < 0.05$).

Visual Image Quality

When 50% of the rays were used, the reconstructed maps for all four algorithms were nearly identical to the reconstructions obtained with the full complement of rays. The reconstructions obtained using the SART algorithm, however,

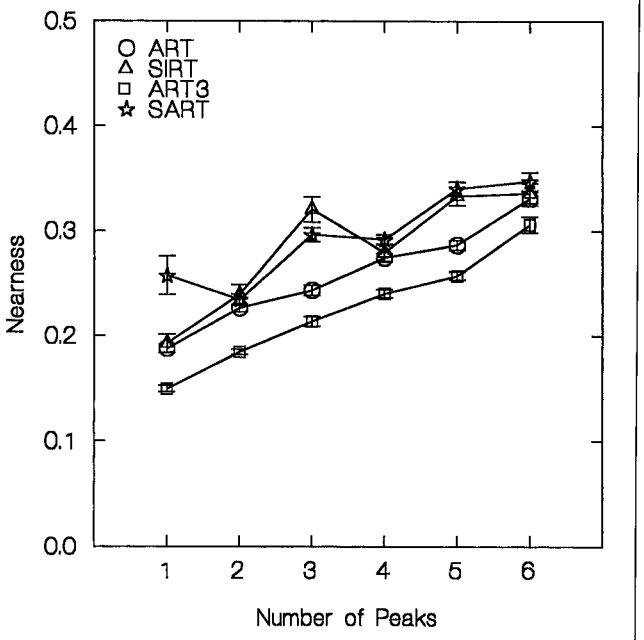

FIGURE 9. Variation of final nearness value with complexity of picture (number of peaks) for the four algorithms with 10% measurement noise; error bars denote one standard error

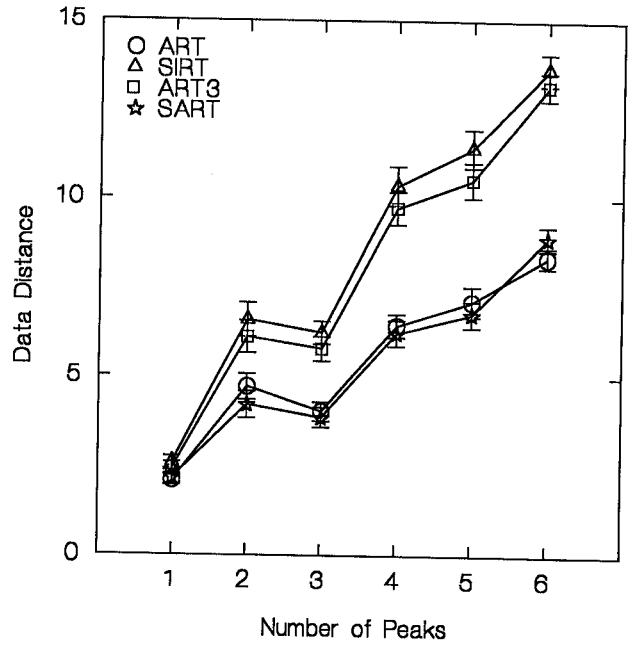

FIGURE 10. Variation of final data distance value with complexity of picture (number of peaks) for the four algorithms with 20% measurement noise; error bars denote one standard error

resulted in the greatest shortening of the tallest and sharpest peaks. When 25% of the rays were used, the reconstructions were close in appearance to the ideal in terms of peak location and shape. However, there was observable degradation in the reconstructions.

Figures 8a, 8b, 8c, and 8d show the reconstructions by the four algorithms when 50% of the rays were used. The reconstructions using ART and SIRT were nearly identical to the reconstructions obtained with the full complement of rays. The peak heights and shapes were essentially unchanged; however, there were additional artifacts evident around the bases of the peaks. SIRT added more artifacts at the base than ART. The reconstruction using SART when 25% of the rays were used was nearly identical to the reconstruction obtained when 50% of the rays were used except for the addition of some artifacts. The reconstruction using ART3 resulted in slightly shortened peaks for the tallest and sharpest peaks; however, the height of the peak at location (16, 35) was increased. This reconstruction using ART3 had more artifacts than the reconstructions using the other algorithms.

Nonideal Sampling Conditions: Noise

Nearness

When noise was introduced into the measurements, the nearness values tended to increase for all algorithms as the number of peaks in the test maps increased. At 5% noise the nearness values for all four algorithms were higher than the ideal case ($p < 0.0001$). There was no statistical difference between ART and ART3, the algorithms with the smallest nearness values. SART had the next largest nearness values, and SIRT had the largest nearness values. This ordering of algorithms from smallest to largest nearness values was identical to the ideal case.

At ± 10% noise the nearness values increased significantly for ART, ART3, and SART ($p < 0.0001$); nearness values were essentially unchanged for SIRT. The order of algorithms from smallest to largest nearness values changed. As shown in Figure 9, ART3 had the smallest nearness values, followed by ART, SART, and SIRT. At this level there was no significant difference between SART and SIRT.

At ± 20% noise the nearness values for all four algorithms were significantly different from one another ($p < 0.0001$). The ordering of algorithms had changed again; SIRT had the smallest nearness values, followed by ART3, SART, and ART.

Data Distance

As the noise level increased, the data distance values increased significantly for each algorithm ($p < 0.001$). The greater the number of peaks in the test maps, the higher the data distance values. At ± 5% noise the order of the algorithms from smallest to largest data distance values was similar to the ideal case: ART had the smallest values, followed by ART3, SART, and SIRT. At ± 10% noise, the order had changed: ART had the smallest data distance values, followed by SART, ART3, and SIRT. At ± 20% noise there was no statistical difference between ART and SART, which had

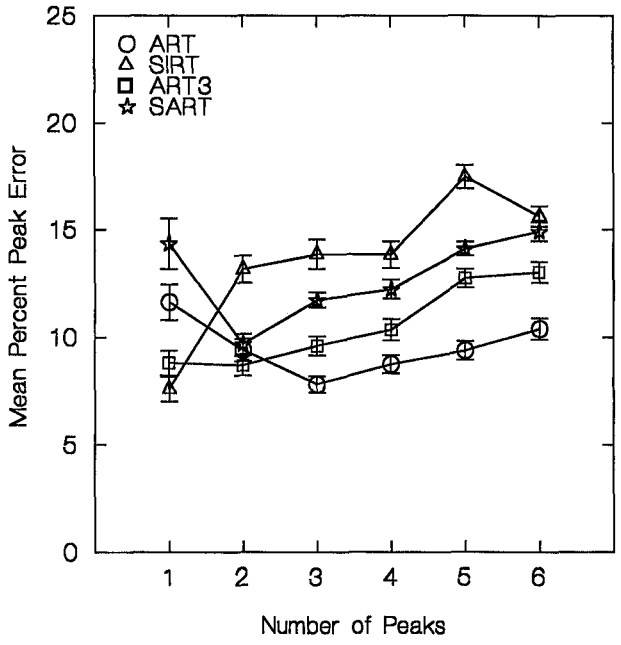

FIGURE 11. Variation of percent error in peak value with complexity of picture (number of peaks) for the four algorithms with 20% measurement noise; error bars denote one standard error

the smallest data distance values (see Figure 10). ART3 had the next highest data distance values, followed by SIRT with the highest values.

Number of Iterations

When noise was added to the simulated measurements, the number of iterations required for convergence decreased for all the algorithms. This was expected because a larger stopping criterion of 0.01 was used. At ± 20% noise, the number of iterations required for convergence was the smallest for ART3, followed by SIRT, ART, and finally SART. At this noise level, the number of iterations required for ART3, SIRT, ART, and SART, dropped from ~10 to 5, ~100 to 7, ~10 to 9, and ~40 to 13, respectively.

Exposure Location Analysis

As the noise level increased, there was a general tendency for the mean percent peak errors to increase for all the algorithms. As the number of peaks in the test maps increased above two, there was a slight increase in the mean percent peak errors for all the algorithms. When the test maps had more than two peaks, the order of algorithms from smallest to largest mean percent errors was the same regardless of noise level; ART had the smallest errors, followed by ART3, SART, and SIRT.

TABLE II. Range of Mean Values for Peak-Centered Errors for Different Levels of Noise

Algorithm	*Ideal*	*± 5%*	*± 10%*	*± 20%*
ART	1.3—9.9	3.4—9.1	4.9—8.9[A]	7.8—10.4[A]
ART3	1.3—9.9	2.8—9.8[A]	4.7—10.6[A]	8.8—13.0[A]
SIRT	4.1—14.7	9.5—15.3[A]	9.5—15.3[A]	9.5—15.3[A]
SART	2.0—11.5	6.26—17.5[A]	6.26—17.5[A]	6.26—17.5[A]

[A] Indicates that the mean value for the peak-centered error is statistically different than the ideal case ($p < 0.0001$)

Figure 11 shows the mean percent peak errors for the four algorithms for the worst-case condition of ± 20% noise. When the test maps had two or more peaks at the ± 5% and ± 10% noise level and three or more peaks at the ± 20% noise level, the ordering of algorithms was similar: ART had the smallest errors, followed by ART3, SART, and SIRT. When the test maps had fewer peaks, there was no consistency in the performance of the algorithms for the different noise levels.

Table II shows the range in mean values for the peak-centered errors for all noise levels. For ART, noise was statistically significant only above the ± 5% noise level ($p < 0.0001$). For ART3, as noise levels increased, the peak errors increased significantly ($p < 0.0001$). For SART and SIRT when noise was added to the measurements, the mean percent error increased significantly above ideal; however, the errors were the same regardless of the particular noise level. For SART at 20% noise the errors were the greatest for the maps with one peak.

For the peak-centered locations, the correlation between the exposure values for the original maps and the reconstructed maps tended to decrease as the percent noise increased for all four algorithms (see Table III). At ± 5%, ± 10%, and ± 20% noise, the correlation was essentially constant for ART and for ART3. The correlation for SIRT was essentially constant regardless of the noise level and was better than the other algorithms at ± 20% noise. The correlation was the poorest for SART at any noise level. As with the

TABLE III. R^2 Values for the Four Algorithms for Different Levels of Noise

		± 5%		*± 10%*		*± 20%*	
Algorithm	*# Peaks*	*Peak*	*Random*	*Peak*	*Random*	*Peak*	*Random*
ART	1—5	0.99	0.99	0.99	0.99	0.97	0.95
	6	0.97	0.97	0.96	0.96	0.92	0.94
ART3	1—5	0.99	0.99	0.99	0.99	0.96	0.95
	6	0.97	0.99	0.96	0.96	0.93	0.94
SIRT	1—5	0.99	0.99	0.98	0.99	0.97	0.98
	6	0.94	0.96	0.94	0.96	0.94	0.95
SART	1—5	0.98	0.97	0.97	0.98	0.96	0.97
	6	0.95	0.95	0.94	0.95	0.90	0.92

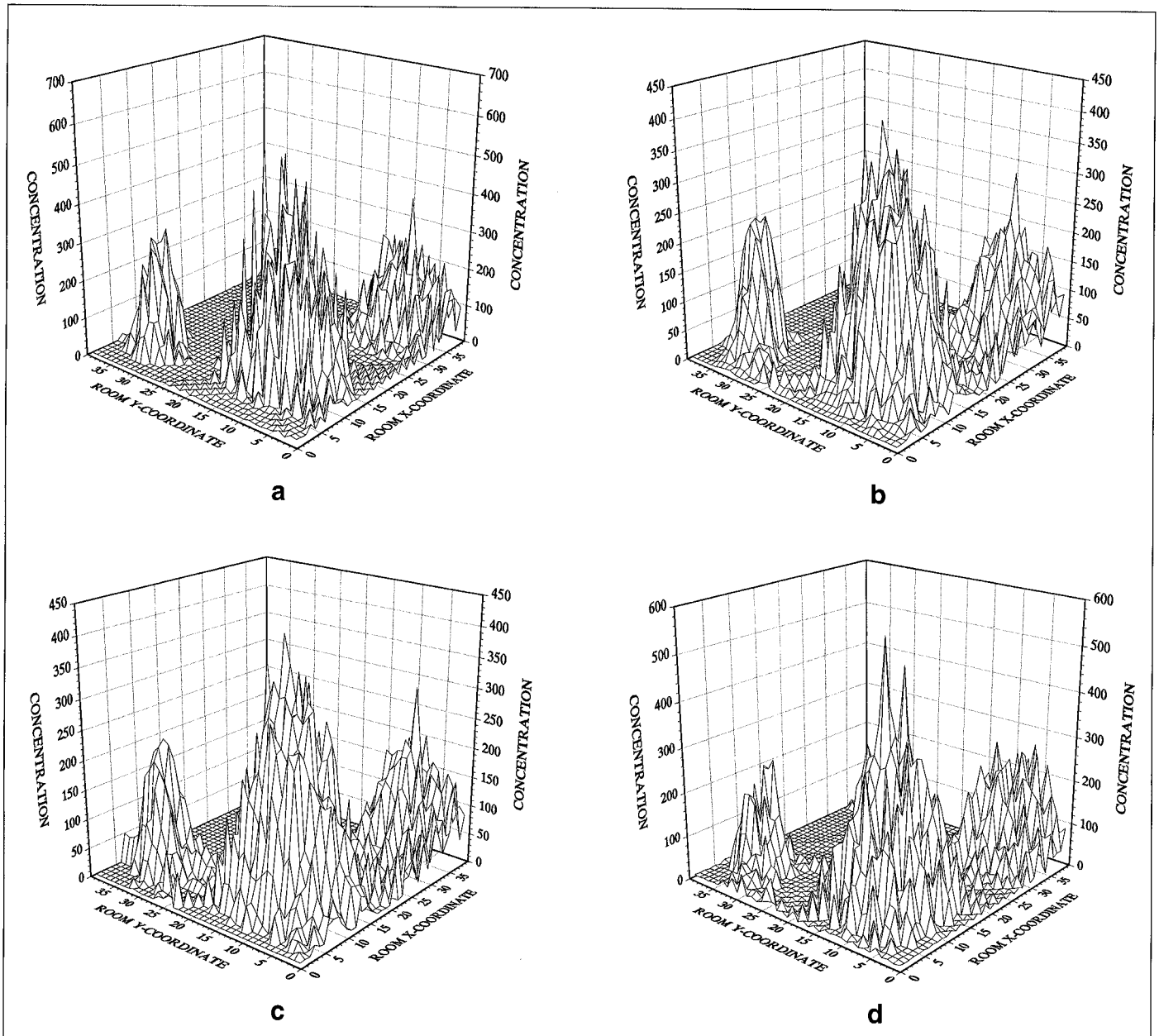

FIGURE 12. Reconstructions with 20% measurement noise using (a) ART; (b) ART3; (c) SIRT; and (d) SART

ideal case, the slopes of the regression lines for the peak-centered errors were all significantly less than 1 ($p < 0.0001$).

The correlation between the exposure values for the original and the reconstructed maps was better for the randomly selected locations than for the peak-centered locations for the test maps with six peaks. For the test maps with fewer than six peaks the correlation was better than the peak-centered values for SIRT and SART and worse for ART and ART3. The slopes of the regression lines for ART and SART were significantly less than 1 for all noise levels. The slopes of the regression lines for SIRT were significantly higher than 1 for all noise levels. The slopes of the regression lines for ART3 were less than 1 for ± 5% noise and greater than 1 for the higher noise levels.

For test maps with three or more peaks the addition of measurement noise resulted in increased errors and decreased correlation for all algorithms; ART gave the best results, SIRT the worst. With the simple test maps with fewer than three peaks, there was no consistency to the performance of the algorithms. For the peak-centered measurements, all of the algorithms underestimated exposure; for the randomly selected locations above 5% noise, ART and SART underestimated exposure, and ART3 and SIRT overestimated exposure.

Visual Image Quality

At ± 5% noise the reconstructions were all similar to one another. They were somewhat peppered with errors, and the shape of the peaks was not as smooth as in the ideal case. At ± 10% noise the reconstructions had deteriorated; the peaks were much more jagged, and additional artifacts were present

at the bases of the peaks, the places of lowest concentration. The ART and ART3 algorithms produced images that were slightly smoother than SIRT and SART.

Figures 12a, 12b, 12c, and 12d show the worst-case reconstructions at ± 20% noise. There were artifacts at the base of the peaks and on the peaks themselves. All three peaks can be identified even at this noise level. ART3 had the smoothest peak reconstructions. ART had peak shapes that looked the noisiest, and the heights of the peaks were increased more than the other algorithms. SIRT added the most artifacts around the base of the peaks, ART added the least.

These images were produced without applying the usual post-reconstruction smoothing procedures. Averaging techniques can decrease the appearance of noise and can result in a better approximation to the original map than can be obtained using an unprocessed noisy picture.[16,28]

CONCLUSIONS

A systematic method has been presented that compares the effectiveness of different algorithms for tomographically reconstructing chemical concentration distributions in air. The underlying assumption is that the performance of an algorithm can be accurately assessed only by thorough testing using a wide variety of possible concentration maps under ideal and nonideal sampling conditions. This research examined 4 different algorithms using 120 different test concentration maps and 6 different sampling conditions. The performance of the algorithms was intimately related to the complexity of the test maps, underscoring the need to use a variety of maps. In addition, more than one reconstruction quality measure should be used to evaluate algorithms; four different criteria were used in this research. It was found that for some sampling conditions, the algorithms were ranked differently depending on the criteria used.

Ideal conditions are important to establish baselines for comparison. Under ideal conditions all the criteria ranked the four algorithms similarly: ART and ART3 were the best, followed by SART and then SIRT.

Ideally, a room is flooded with contiguous parallel rays; the optimal ray widths are $(1/N)\max\{|\sin\theta|, |\cos\theta|\}$, where N is the number of grid cells on one side of the room, and θ is the projection angle.[15,19] In practice, there may be physical and cost limitations to obtaining a large number of projection data. The simulations using a reduced number density of rays were performed to examine this. Three of the algorithms had little alteration in reconstruction quality with only 50% of the rays, when compared to the ideal case; the performance of SART deteriorated by all criteria. When only 50% of the rays were used, the algorithms were ranked the same by each of the reconstruction quality measures. When 25% of the rays were used, all of the algorithms had decreased reconstruction quality. Based on exposure location errors and nearness, the algorithms were the same; however, there were visual differences. The algorithms differed in the introduction of artifacts at the bases of the peaks and the amount of shortening of the peak heights. Visually, ART gave the best reconstructions, ART3 the worst. If quantitative measures were the only ones used to evaluate image quality, the algorithms would have appeared alike.

The visual and quantitative impact of reducing the number density of rays is greatest when the concentration peaks are closer to one another than the rays, or when the rays do not pass through the highest concentration points. Other research has shown that when setting up a remote sensing configuration, if possible, the rays should be positioned near the expected points of highest concentration.[29]

When simulated measurement noise was added, the performance of each algorithm deteriorated. ART and ART3 were stable at low levels of noise; as the noise level increased above ± 5%, performance deteriorated with increasing noise. SIRT and SART were sensitive to low levels of noise; performance deteriorated at ± 5% noise, and was stable as noise increased.

Discrepancies among the quantitative image quality measures were particularly obvious at ± 20% noise. Among the algorithms SIRT had the smallest nearness values, the highest data distance values, the highest mean peak errors for test maps with greater than two peaks, and the lowest mean peak errors for maps with one peak. Within algorithms there were discrepancies between nearness trends and mean peak location errors. For ART and SART, maps with one peak had the largest mean peak errors, and the smallest nearness values. Nearness is a global measure of accuracy for the entire map, while mean peak error is a local measure and focusses only on the points of highest concentration; therefore, the results would not necessarily follow the same trends.

The exposure location error analysis was very useful for comparing the algorithms for accuracy of exposure assessment. Two types of measurements were calculated: worst-case peak-centered and randomly located. The peak-centered measurement consistently underestimated exposures; the randomly located measurement gave better exposure estimates, and for some test conditions, over-estimated exposures. This over-estimation was probably due to the addition of artifacts at the bases at the peaks that would increase values over background. In future studies, the peak-centered measurement could be used alone as a worst-case analysis of peak height reduction.

Both nearness and data distance should be used when evaluating algorithms because they are different measures of reconstruction quality. Nearness evaluates the overall reconstructed image, data distance evaluates how close the reconstructed ray sums are to the measured ray sums. These measurements ranked the algorithms similarly for the ideal case, and for the reduction in the number density of rays; however, they ranked the algorithms differently in the presence of measurement noise. Nearness is only a research tool, it cannot be used for experimental verification because it requires knowledge about the true concentration map. In contrast, data distance can be used for experimental verification.

The number of iterations required for convergence was similar for ART, ART3, and SART for nonideal sampling conditions. SIRT took the most iterations. Number of iterations relates directly to convergence rate, not to computation

time. SART was the most computationally expensive algorithm and took the longest time for convergence.

Two important conclusions were reached from this research. First, as echoed by other authors, algorithms need to be tested using images and sampling configurations specific to the application in which they will be used. Second, when evaluating algorithms, the choice of the algorithm will depend on the ultimate purpose of the tomographic reconstructions.

Algorithms tested for other applications may use different configurations, a different number of projections, and different types of test images. The majority of algorithms have been tested for medical applications, and some have been tested using a photograph of a person or geometric patterns.

These images are very different from chemical concentration gradients. Most of the studies in the literature have used a far greater number of projections than used in this research. Given these differences, it was not altogether surprising that the results presented here for reconstructing chemical concentrations did not always agree with the results found in the literature using the same algorithms in other disciplines.

Other research found that SIRT was superior to ART and ART3 based on visual assessment and nearness when reconstructing circles of uniform density[21] and based on visual assessment when reconstructing a beating heart from X-ray measurements using 10% noise.[20] This research found ART and ART3 to be better than SIRT based on both measures for the same noise level. For reconstructing a "head phantom," which consists of a number of ellipses of various densities, other research found that SART was more resistant to the effects of noise than the other ART algorithms;[23] this research found it to be worse than ART when noise was used.

When evaluating algorithms for computer tomographic reconstruction of chemical concentrations in air from a remote sensing system, the eventual use of the system must be considered. Reconstruction quality criteria should be related directly to the problem to be solved. For example, if the system is only to be used for leak detection of chemicals, where location of peaks is more important than absolute concentration, any of the algorithms could be used. All of them reconstructed the peaks in the correct locations. If the system is to be used for exposure assessment information, then absolute peak height is important; algorithms that do not substantially smooth out the peaks (like ART or ART3) should be chosen. In this study, using four projections, ART resulted in the least reduction in peak height. If smaller reductions in peak height are necessary, additional projection angles must be added. If the system is to be used for evaluating the air flow of contaminants through a room, evaluating a ventilation system, or validating fluid flow models, then overall accuracy and suppression of artifacts would be important. ART3 might be a good choice here.

Computer tomographic reconstructions of concentrations of air contaminants using an optical remote sensing system shows promise as a method to produce two-dimensional concentration maps of an entire room with good spatial and good temporal resolution. For this research, as few as 120 rays were used to reconstruct 1600 cells in a 40 × 40 room. This is obviously far fewer than would be needed to get the same level of spatial detail using the traditional point sampling methods. Tomography also offers a gain in efficiency for determining many points in a room; the number of required beam paths increases slowly compared to the number of reconstructed points in the sampling grid. For example, if the room were an 80 × 80 grid instead of a 40 × 40 grid, the number of cells in the room would quadruple while the number of rays required would double. The near real-time measurement capability of a remote sensing system coupled with the ability to reconstruct the concentration maps in a matter of minutes would result in good temporal resolution.

The success of the system in practice will depend on the reconstruction algorithm, configuration, and remote sensing equipment. This article dealt with the evaluation of algorithms using numerical studies. For studies like this, the usefulness of the results is highly dependent on the realism of the simulations. Therefore, evaluation should include all measurement uncertainties. Uncertainties not measured here include errors in the measurement of the projection angles in the configuration, and the relationship between instrument scan time, or the time required to take all the projections, and air movement in the room. Slight errors in the measurement of angles could either be systematic or random. The relationship between scan time, air movement, and accuracy is not simple to predict. Because concentrations of pollutants in indoor air are rarely in steady state, the amount of scan time must be balanced with the movement of air contaminants to obtain the best reconstructions; the longer the scan time, the more movement of contaminants, and, therefore, the more inconsistencies in the projection data. Work is currently underway to evaluate these additional uncertainties, as well as alternative configurations.

ACKNOWLEDGEMENT

The authors would like to thank Robert Katz for his invaluable technical assistance to this project.

REFERENCES

1. **Corn, M.:** Strategies of Air Sampling. *Scand. J. Work Environ. Health.* 11:173–180 (1985).
2. **Todd, L.A. and D. Leith:** Remote Sensing and Computed Tomography in Industrial Hygiene. *Am. Ind. Hyg. Assoc. J.* 51:224–233 (1990).
3. **Herget, W. and J. Brasher:** Remote Fourier Transform Infrared Air Pollution Studies. *Opt. Eng.* 19:508–514 (1980).
4. **Grant, W.B. and R. Menzies:** A Survey of Laser and Selected Optical Systems for Remote Measurement of Pollutant Gas Concentrations. *J. Air Pollution Cont. Assoc.* 33(3):187–194 (1983).
5. **Xiao, H.K., S.P. Levine, W.F. Herget, J.B. D'Arcy, R. Spear, and T. Pritchett:** A Transportable, Remote Sensing, Infrared Air Monitoring System, *Am. Ind. Hyg. Assoc. J.* 52:449–457 (1991).

6. **Hounsfield, G.N.:** Computerized Transverse Axial Scanning (Tomography): Part I. Description of a System. *Br. J. Radiol. 46*:1016–1022 (1973).
7. **Bracewell, R.N.:** Strip Integration in Radio Astronomy. *Aust. J. Phys. 9*:198–217 (1956).
8. **DeRosier, D.J. and A. Klug:** Reconstruction of Three-Dimensional Structures from Electron Micrographs. *Nature 217*:130–134 (1968).
9. **Wolfe, D.C. and R.L. Byer:** Model Studies of Laser Absorption Computed Tomography for Remote Air Pollution Measurement. *Appl. Optics 21(7)*:1165–1177 (1982).
10. **Gordon, R. and G.T. Herman:** Three-Dimensional Reconstruction from Projections: A Review of Algorithms. In: *International Review of Cytology,* ed. by G.H. Bourne and J.F. Danielli. New York: Academic Press (1974). pp. 111-151.
11. **Hanson, K.M.:** Method of Evaluating Image-Recovery Algorithms Based On Task Performance. J. Opt. Soc. Am. A. 7(7):1294–1304 (1990).
12. **Cormack, A.M.:** Representation of a Function by Its Line Integrals, with Some Radiological Applications. *J. Appl. Phys. 34*:2722–2727 (1963).
13. **Cormack, A.M.:** Representation of a Function by Its Line Integrals, with Some Radiological Applications. II. *J. Appl. Phys. 35*:2908–2913 (1964).
14. **Kuhl, D.E. and R. Edwards:** Image Separation Radioisotope Scanning. *Radiology 80*:653–661 (1963).
15. **Brooks, R.A. and G. Di Chiro:** Principles of Computer Assisted Tomography (CAT) in Radiographic and Radioisotopic Imaging. *Phys. Med. Biol. 21*:689–732 (1976).
16. **Gordon, R., R. Bender, and G.T. Herman:** Algebraic Reconstruction Techniques (ART) for Three-Dimensional Electron Microscopy and X-ray Photography. *J. Theor. Biol. 29*:471–481 (1970).
17. **Brooks, R.A. and G. Di Chiro:** Theory of Image Reconstruction in Computed Tomography. *Radiology 117*:561–572 (1975).
18. **Oppenheim, B.E.:** Reconstruction Tomography from Incomplete Projections. In *Reconstruction Tomography in Diagnostic Radiology and Nuclear Medicine, ed. by* M. Ter-Pogossian. University Park Press (1977).
19. **Herman, G.T., A. Lent, and S.W. Rowland:** ART: Mathematics and Applications. A Report on the Mathematical Foundations and on the Applicability to Real Data of the Algebraic Reconstruction Techniques. *J. Theor. Biol. 42*:1–32 (1973).
20. **Herman, G.T.:** A Relaxation Method For Reconstructing Objects From Noisy X-Rays. *Math. Programming 8*:1–19 (1975).
21. **Gilbert, P.:** Iterative Methods for the Three-dimensional Reconstruction of an Object from Projections. *J. Theor. Biol. 36*:105–117 (1972).
22. **Andersen, A.H. and A.C. Kak:** Digital Ray Tracing in Two-Dimensional Refractive Fields. *J. Acoust. Soc. Am. 72*:1593–1606 (1982).
23. **Andersen, A.H. and A.C. Kak:** Simultaneous Algebraic Reconstruction Technique (SART): A Superior Implementation of the ART Algorithm. *Ultrasonic Imaging 6*:81–94 (1984).
24. **Andersen, A.H.:** Algebraic Reconstruction in CT from Limited Views. *IEEE Trans. Med. Imaging 8(1)*:50–55 (1989).
25. **Herman, G.T. and S. Rowland:** Three Methods for Reconstructing Pictures from X-Rays: A Comparative Study. *Comput. Graph. Image Proc. 1*:151–178 (1973).
26. **Gordon, R.:** A Tutorial on ART. *IEEE Trans. on Nuc. Sci. NS-21*:78–93 (1974).
27. **Todd, L.:** Optical Remote Sensing/Computed Tomography Systems for Workplace Exposure Assessments. In *Proceedings Optical Remote Sensing Applications to Environmental and Industrial Safety Problems. AWMA.* 356–360 (1992).
28. **Frieder, G. and G.T. Herman.** Resolution in Reconstructing Objects from Electron Micrographs. *J. Theor. Biol. 33*:198–211(1971).
29. **Todd, L.** "Optical Remote Sensing and Computed Tomography in Industrial Hygiene." Ph.D. diss. University of North Carolina, Chapel Hill, N.C. (1990).